Volume 70, Issue 2, 2026
Journal of Scientific Research
of
The Banaras Hindu University

Advancing in Self-Powered Optoelectronics: High-Speed Photodetection with FTO / nc-CdS: Ag 3% Heterojunction

Baljinder Singh*1, and Krishan Kumar[2]

*1Associate Professor, Department of Physics, S. D. (PG) College, Panipat-132103, Haryana, India,
Email: sbaljindr@gmail.com
[2]Associate Professor, Department of Physics, Sanatan Dharma College, Ambala Cantt. -133001, Haryana, India,
Email:kkmajra@gmail.com

Abstract: **The successful development of a self-powered, high-speed photodetector using the FTO/nc-CdS: Ag 3% heterojunction marks significant progress in optoelectronics. This was achieved by depositing silver-doped nanocrystalline cadmium sulfide (nc-CdS: Ag 3%) thin films onto a fluorine-doped tin oxide (FTO) coated glass substrate through thermal evaporation using the Inert Gas Condensation (IGC) method. The device operates entirely without external power, displaying excellent rectification properties in darkness and a clear photovoltaic response when illuminated. It exhibits rectification with a ratio of 41.73 within ±2.4 V in the dark. Photoconductive tests show that the device is highly sensitive to light and responds rapidly. The rise and fall times measured are around 286 µs and 270 µs, respectively. With possible applications in light-sensitive technologies, this self-powered photodetector with high speeds is promising for future improvements in optoelectronics.**

Index Terms: **Inert Gas Condensation, Nanocrystalline, Optoelectronics, Photodetector, Rectification.**

I. Introduction

The growing demand for efficient and long-lasting energy solutions around the world has led to more attention on self-powered energy devices [1]. These devices collect energy from their surroundings, like sunlight, body heat, or movement, without needing a separate power supply. They work well in areas like wearable electronics, connected devices in the Internet of Things (IoT), and systems that monitor environments from a distance. Among them, self-powered photodiodes, particularly heterojunction-based ones, have emerged in prominence because of their high sensitivity, rapid response, and the fact that they can function without being externally biased, showing tremendous performance in optoelectronics.

The performance of self-powered Schottky diodes, including rectification efficiency, photoresponse speed, wavelength sensitivity, mechanical durability, and flexibility, is primarily determined by the choice of semiconductor material and the design of the other conductive material contact. Silicon is well known for being highly efficient at converting energy and reliable [2]. In the visible and ultraviolet (UV) light ranges, materials like cadmium sulfide (CdS) and zinc oxide (ZnO) exhibit strong responses to light [3]. Organic semiconductors are very stretchable [4], making them ideal for use in wearable devices. Graphene is flexible and can detect a wide range of light frequencies very quickly [5]. Additionally, conductive metal-organic frameworks (MOFs) and hybrid nanostructures enable the development of customizable, multifunctional devices [6]. The best material to use depends on the specific requirements of the target application, such as speed, spectral sensitivity, mechanical robustness, and environmental stability.

Cadmium sulfide (CdS) is a type of II-VI semiconductor that has a direct bandgap of around 2.4 eV. It is widely recognized for its excellent optoelectronic properties, such as high optical transparency, photoconductivity, and good electron mobility. Because of these characteristics, CdS is often considered a strong candidate for applications in photodetectors, solar cells, and light-emitting diodes. To prepare high-quality CdS thin films, researchers have looked into various deposition methods like chemical bath deposition [7], Close Spaced Sublimation (CSS) [8], and vacuum evaporation [9]. In our research, we use vacuum evaporation to deposit 3% Ag-doped CdS thin films onto FTO substrates. This process ensures uniform thickness of the film with high quality, allowing better structural and optoelectronic performance of the resultant device.

* Corresponding Author

In this article, we examine the structure and light-related electrical properties of the FTO/nc-CdS: Ag 3% Schottky diode, focusing on its operation without an external power source and its response time to light. Adding silver doping is aimed at increasing the device's sensitivity to light while keeping the CdS crystal structure unchanged. We examine the crystallographic structure, surface morphology, and optical absorption of the CdS films, as well as the opto-electrical properties of the Schottky junction. In addition, we explore the potential applications of this device in future high-speed optoelectronic devices, including photodetectors and energy-efficient sensors, and its contribution to the next-generation self-powered technologies.

II. Experimental

The melt quenching method was employed to make the silver-doped CdS material. High-purity elements were accurately measured and put into quartz ampoules based on the atomic percentages of each component. A vacuum level of 2×10^{-5} mbar was kept during the sealing process. The sealed ampoules were then placed in a furnace, where the temperature was slowly raised to 1200°C at a rate of 2 to 3 °C per minute [10].

The ampoules were held at this maximum melting point temperature for 24 hours to achieve a homogeneous melt. Quenching was executed by immersing the sealed ampoules in ice-cold water. The thermal vacuum evaporation process was carried out using a vacuum coating unit (HINDHIVAC, MODEL: VS-65). The thin films are deposited on well-degassed transparent fluorinated tin oxide (FTO) glass substrates using the inert gas (Ar) condensation (IGC) technique. This entire process was conducted at a base pressure of 2×10^{-5} mbar and at room temperature. To ensure thermodynamic equilibrium, the thin films were kept within the deposition chamber in the dark for 24 hours before measurements were taken. A Scanning Electron Microscope (FE-SEM) (MODEL: HI-0876-0003) was used to study the FE-SEM graphs. The structural parameters of nc-CdS: Ag 3% samples were estimated by X-Ray Diffraction (XRD) using a Spinner 3064 XPERT-PRO X-Ray diffractometer (CuKα =1.54056 Å) at a scanning speed of 0.02° s^{-1} in the 2θ range from 20° to 70° [9]. Raman spectra were recorded with a Spex Model Ramalog 1403 double monochromator equipped with an RCA 31034A photomultiplier tube [11]. Optical absorption and

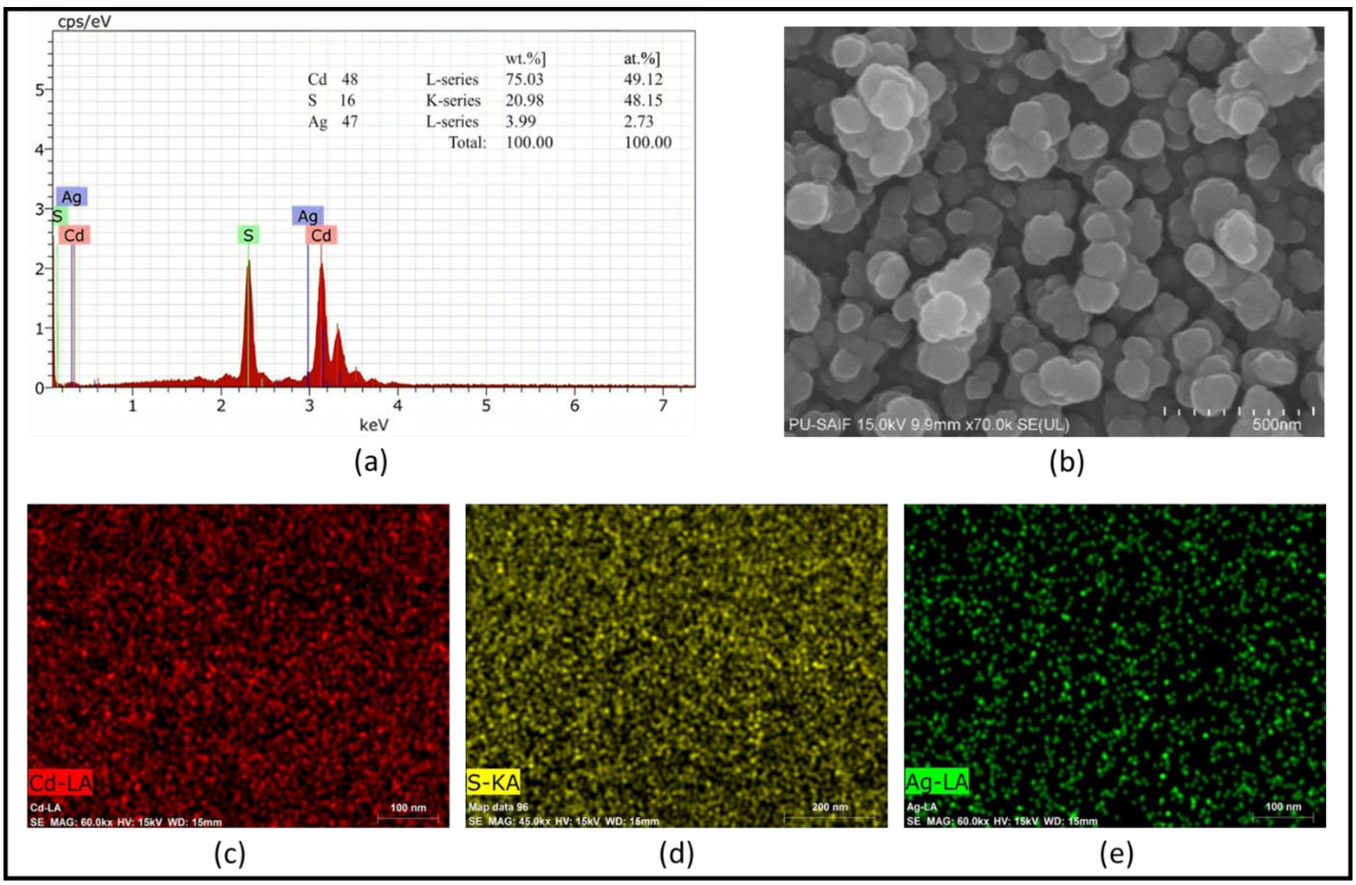

Fig. 1. EDAX spectra and FE-SEM image of nc-CdS: Ag 3% thin film. Panel (c-e), the Cd, S, and Ag are evenly spread throughout the nc-CdS: Ag 3% thin film.

transmission measurements were carried out in a UV/VIS/NIR computer-controlled spectrophotometer (Perkin Elmer LAMBDA 750) in the transmission range from 300 nm to 2500 nm at room temperature (300 K). Ag point contacts (~1 mm²) were formed using silver paste on both the exposed FTO substrate and the top surface of the nc-CdS: Ag film, ensuring stable electrical connections while preserving the integrity of the device's heterojunction. Electrical characterization was performed by current-voltage (I-V) measurements under dark and illuminated conditions using a Keithley electrometer 6517A as the voltage source. Photoconductive response times were assessed using a modulated light source and oscilloscope setup. To improve signal-to-noise ratio, samples were placed in a specially designed metallic sample holder. A Digital Phosphor Oscilloscope (MODEL: Tektronix DPO 4054, interfaced via Tekvisa software) was utilized to record the electric current produced in the absence of an external electric field [9].

III. Results and Discussion

The purity and exact makeup of the Ag-doped nc-CdS thin film were checked using EDAX, which confirmed the presence of cadmium (Cd), sulfur (S), and silver (Ag) as the elemental components. The typical EDAX spectra for the nc-CdS: Ag 3% are presented in Fig. 1 (a). Additionally, the quantitative atomic percentages of the compositional elements Cd, S, and Ag found in the thin films are provided as an inset in Fig. 1 (a). FE-SEM is an effective technique for studying the surface morphology of thin films, offering valuable insights into the shape and size of the grains. Fig. 1 (b) shows the FE-SEM micrograph of the nc-CdS: Ag 3% thin film. The observations from this micrograph indicate that the deposited film is homogeneous, with spherical grains that uniformly cover the FTO-coated glass substrate (Fig. 1). Notably, the absence of cracks or pinholes in the micrograph is a positive indication of the film's quality [9].

Fig. 2(a) shows the XRD pattern for both the FTO-coated glass substrate and the nc-CdS: Ag 3% thin film deposited on FTO-coated glass substrate at 300 K. The pattern for the FTO substrate closely matches the standard pattern for cubic phase SnO_2 (JCPDS No. 41-1445) [12]. The nc-CdS: Ag 3% thin film deposited on FTO-coated glass substrate exhibits diffraction peaks attributed to both CdS and FTO. Along with the diffraction peaks from the FTO, the nc-CdS: Ag 3% thin film displays peaks at 2θ values of 25.54°, 26.56°, 28.40°, and 48.11°. These peaks correspond to the (100), (002), (101), and (103) reflections of the hexagonal phase of CdS, as indicated by JCPDS card No. 06-0314. This confirms the polycrystalline nature of the thin film, with a preferential growth direction along the (002) plane. All diffraction peaks are well indexed, and no impurity phases were detected, indicating a high phase purity of the deposited film. There are no additional peaks corresponding to Ag_2S or other phases [9]. The interplanar spacing for the (002) plane, denoted as d_{002}, is calculated using the relation $\lambda = 2d_{002} \sin\theta$, yielding a value of 3.36 Å. The crystallite size (D) for the predominant (002) peak is calculated using Debye-Scherrer's formula: $D = 0.94\lambda / (\beta \cos\theta)$, where θ is the Bragg's diffraction angle, λ (~1.54 Å) is the wavelength of the X-ray, and β is the full width at half maxima (FWHM) in radians. The calculated crystallite size D is found to be 31 nm. The micro-strain (ε) is estimated using the formula $\varepsilon = \beta \cos\theta / 4$, with a resulting value of 0.00116 $Lines^{-2}\ m^{-4}$ [13].

The Raman spectra of the nc-CdS: Ag 3% and nc-CdS thin films are displayed in Fig. 2(b). It is evident that two significant peaks appear at 289 cm^{-1} and 585 cm^{-1} in both the nc-

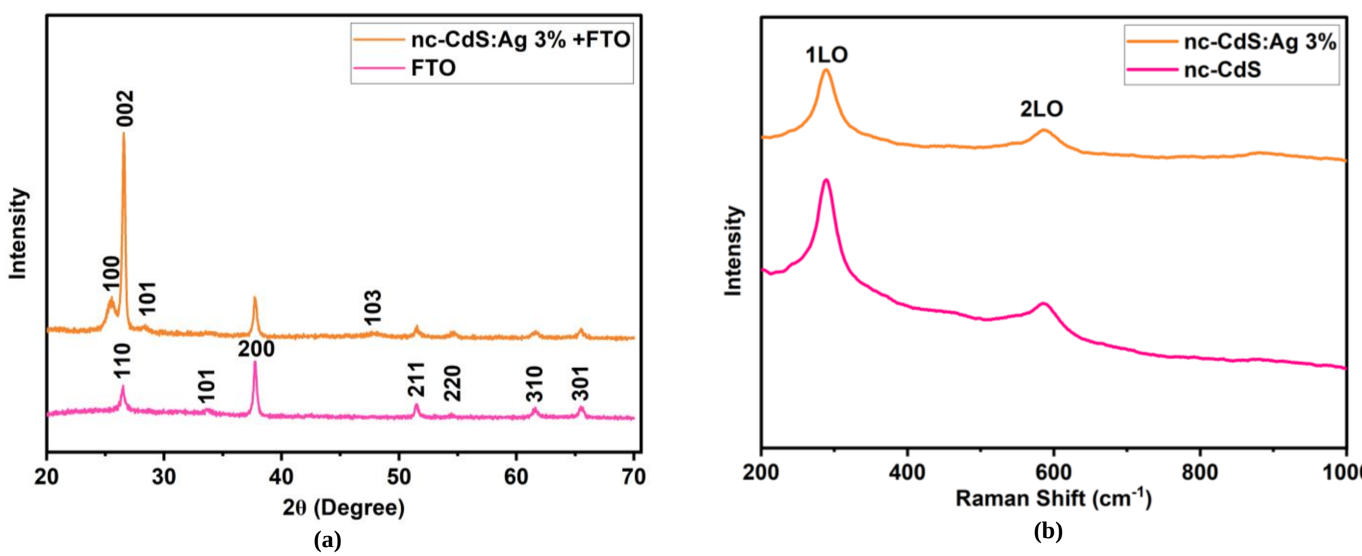

Fig. 2. X-ray diffraction patterns of FTO-coated glass substrate and nc-CdS: Ag 3% thin film deposited on FTO-coated glass substrate. **(b)** Typical Raman spectrum of nc-CdS: Ag 3% and nc-CdS thin films.

.

CdS: Ag 3% and the nc-CdS thin films deposited at room temperature. These peaks correspond to the first and second-order longitudinal optical (LO) phonon modes of CdS, respectively [14]. This indicates that the nc-CdS: Ag 3% thin film has a crystal structure similar to that of bulk CdS.

The optical transmission spectra, covering the wavelength range from 300 nm to 2500 nm, of the nc-CdS: Ag 3% thin film, which was deposited at room temperature, 300 K, are shown in Fig. 3. The relationship between transmittance (T) and the absorption coefficient (α) is described by the Lambert-Beer law:

$$T = e^{-\alpha d}$$

For direct-band semiconductors, the band gap (Eg) is related to the absorption coefficient through the 'Tauc' relation [15]:

$$h\nu\alpha = A(h\nu - E_g)^{\frac{1}{2}}$$

In this case, h stands for the Planck constant, ν represents the photon frequency, and A is a characteristic parameter that doesn't depend on the energy of the photon. To find the band gap (E_g), we look at the straight part of the graph that shows $(h\nu\alpha)^2$ versus hν and extend it to where α equals zero (as shown in the inset of Fig. 3). The optical band gap for the nc-CdS: Ag 3% thin film is 2.21 eV, which is smaller than the band gap of regular CdS, which is 2.42 eV. This indicates a red shift in the optical band gap for the CdS: Ag 3% thin films compared to bulk CdS. During the preparation of thin films from the doped material, a significant number of defects such as vacancies, interstitials, dislocations, and strain can be introduced. These defects, which may act as trap centres, play a crucial role in influencing optical absorption. As a result, the observed reduction in the optical band gap is mainly due to defect-induced band tailing, which occurs because of the presence of localised energy states near the band edges [16].

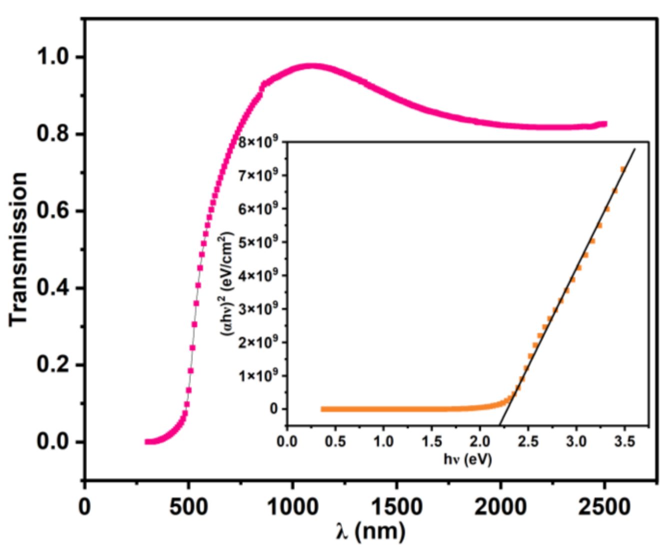

Fig. 3. Optical transmission spectra of the nc-CdS: Ag 3% thin film measured at room temperature. The inset shows the plot between $(h\nu\alpha)^2$ and hν for the nc-CdS: Ag 3% thin film.

The photodetector's spectral response was studied by measuring its sensitivity across different incident wavelengths, as illustrated in Fig. 4. The sensitivity curve demonstrates a pronounced peak, with maximum sensitivity observed at approximately 560 nm. This wavelength matches the bandgap of CdS, meaning the photo-response mainly results from direct band-to-band electron excitations. The detector exhibits

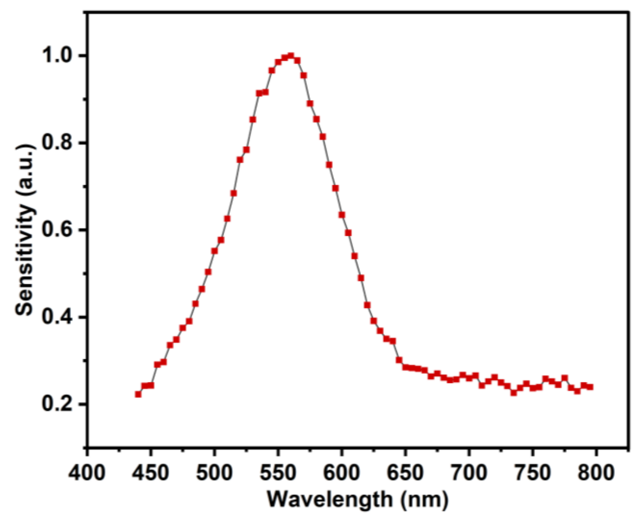

Fig. 4. Spectral sensitivity of nc-CdS: Ag 3% thin film photodetector.

significant responsivity over a range spanning from about 450 nm to 650 nm, defining its effective operational range. Below 450nm and above 700nm, the sensitivity rapidly decreases and approaches baseline levels. This indicates that the photodetector is optimally suited for light detection in the visible spectrum, with the highest efficiency near the green region [17-18].

Fig. 5 shows the I-V curves of the device, measured under both dark conditions and white light with light intensities of 3.6 mW cm^{-2} and 8.5 mW cm^{-2}. It's clear that the current flowing through the device increases when light is applied, and the current continues to rise as the light intensity increases. The device exhibits rectification characteristics, achieving a rectification ratio of 41.73 within a voltage range of ±2.4 V. For an ideal diode, the relationship between current (I) and voltage (V) can be expressed using the following equations [18-19]:

$$I = I_0\left\{e^{\frac{q(V-IR_S)}{nK_BT}} - 1\right\}$$

$$I_0 = AA^*T^2 exp\left(\frac{-q\Phi_B}{K_B T}\right)$$

Where I_0 is the reverse saturation current, R_s is the series resistance, n is the ideality factor, K_B is Boltzmann's constant, T is the temperature in Kelvin, A is the area of the Schottky contact, A* is the Richardson's constant (which is about 24 A K^{-2} cm^{-2} for CdS), and Φ_B is the barrier height. To estimate the series resistance (R_s), we can focus on the high-current region where it dominates. The slope of the voltage (V) versus current (I) graph in the forward bias region (V > 2V) reveals that the value of R_s is 20 kΩ. The ideality factor (n), extracted from the slope of the natural logarithm of current (ln I) versus voltage (V), is found to be 9.5, which is significantly higher than the ideal value of 1-2 expected for a perfect Schottky diode. This elevated ideality factor indicates non-ideal behavior, which can be attributed to a combination of factors such as interface states, defects within the nanocrystalline film, and series resistance effects [17, 20].

Nanocrystalline CdS films typically contain a high density of trap states and grain boundaries that act as recombination centers, which degrade the ideal diode behavior by introducing additional recombination and tunneling pathways. These effects increase the ideality factor as reported in several studies on Schottky and heterojunction photodetectors employing CdS and other wide bandgap materials [21-22]. The series resistance, experimentally estimated to be approximately 20 kΩ, also contributes to the deviation from ideality by introducing voltage drops internal to the device.

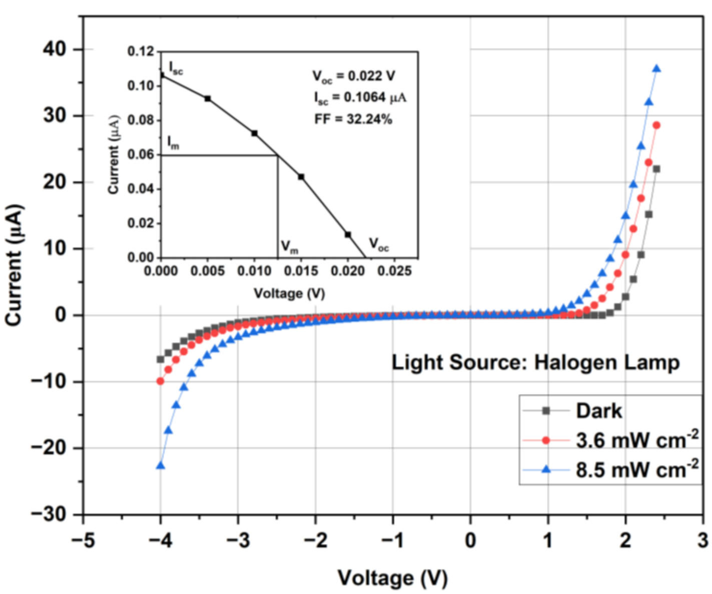

Fig. 5. I-V characteristics of FTO/nc-CdS: Ag 3% Schottky diode heterojunction measured in dark and under light illumination of different intensities. The inset shows the photovoltaic characteristics of the FTO/nc-CdS: Ag 3% Schottky diode heterojunction under halogen light illumination with an intensity of 8.5 mW/cm².

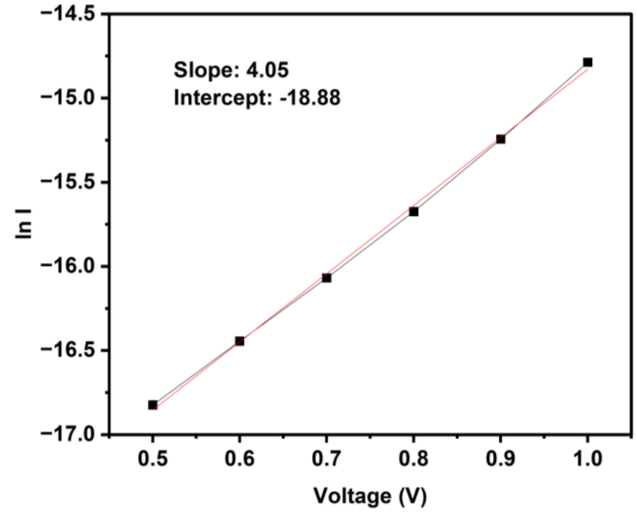

Fig. 6. ln I-V plot under forward-bias condition.

Such non-idealities are common in nanostructured semiconductor devices and do not necessarily preclude high-performance photodetection. Rather, they highlight the complexity of charge transport mechanisms in doped nanocrystalline materials. The high ideality factor observed aligns with previous reports on similar CdS-based photodetectors, where values in the range of 4 to 10 have been recorded due to interface and defect contributions [23-25]. Further optimization of film quality and interface engineering could reduce these effects, potentially lower the ideality factor and enhance device efficiency.

Additionally, the reverse saturation current (I_0) was estimated to be 6.2×10^{-9} A, and the Schottky barrier height (Φ_B), calculated using the relevant equation, was found to be 0.866 eV. The combination of a high barrier height and a relatively low leakage current demonstrate good junction quality and efficient charge transport, reinforcing the potential of the FTO/nc-CdS:Ag 3% heterojunction device for photodetector applications with desirable rectifying and photosensitive properties.

The device demonstrates photovoltaic properties, with an open-circuit voltage (V_{oc}) of 0.022 V and a short-circuit current (I_{sc}) of 0.1064 μA (as shown in the inset of Fig. 5). In the voltage range from 0 to V_{oc}, the current decreases approximately linearly as the voltage increases. The maximum power output is calculated to be 0.75 nW, which occurs at a voltage (V_m) of 0.013 V and a current (I_m) of 0.06 μA. As a result, the fill factor (FF), defined as FF = (V_m * I_m) / (V_{oc} * I_{sc}), is 32.24% [26].

The performance of a photodetector can be assessed using three main factors: sensitivity (S), responsivity (R), and relative detectivity (D*). Sensitivity (S) shows how much the current increases when the detector is exposed to light. It is commonly used to show how much the signal improves or how much the photocurrent increases compared to the dark current. Responsivity (R) refers to the amount of photocurrent produced for each unit of light power that hits the detector's surface area. Relative detectivity (D*) indicates the smallest detectable optical signal that the photodetector can identify. These metrics are essential for assessing how effectively a photodetector can convert light into an electrical signal [27-28].

$$S = \frac{(I_p - I_d)}{I_d}$$

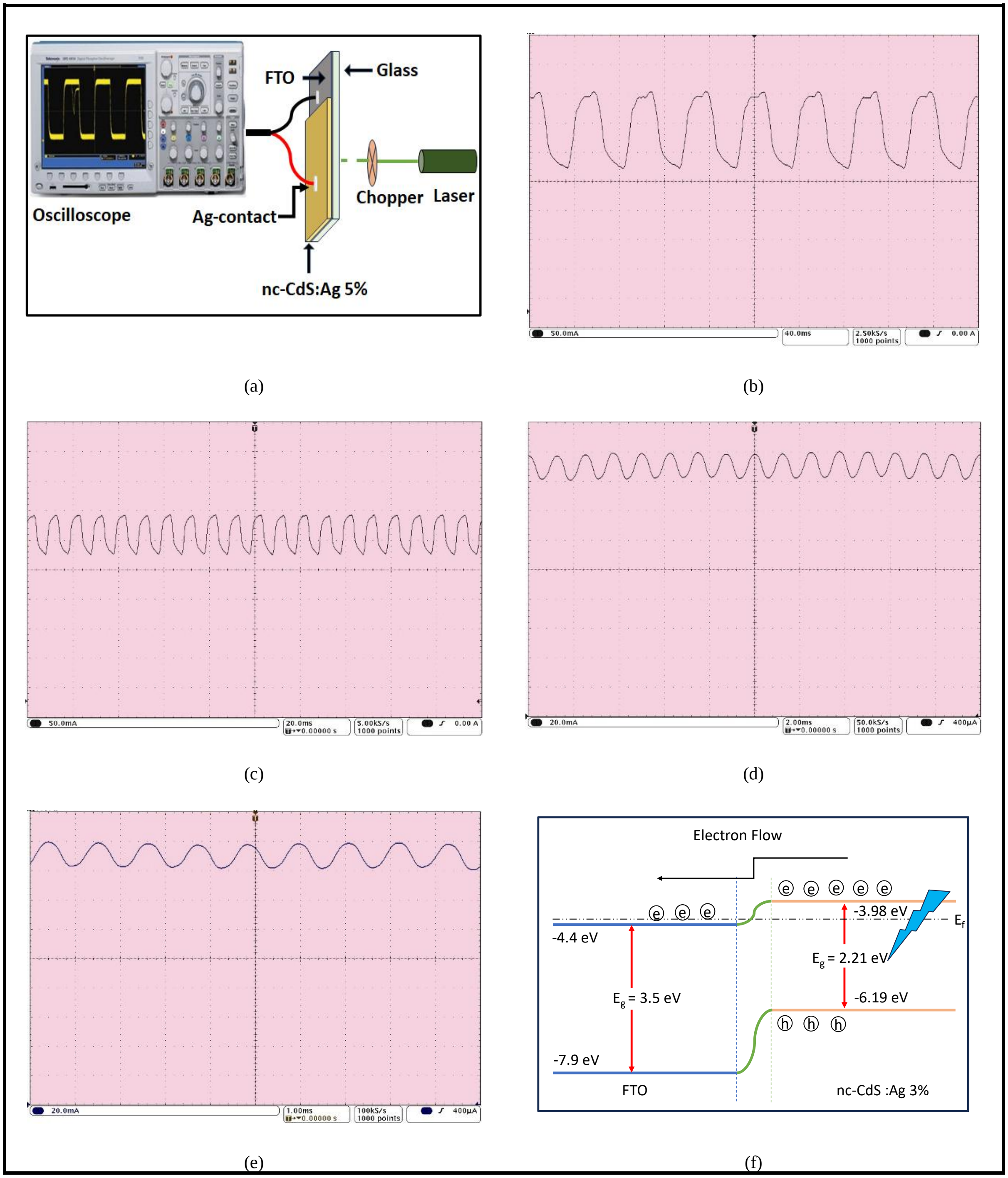

Fig. 7. Schematic illustration of our experimental set-up for photoresponse detection. Photoresponse characteristics of the FTO/nc-CdS: Ag 3% device to pulsed light irradiation at frequency (b) 20 Hz, (c) 100 Hz, (d) 800 Hz, and (e) 1000 Hz. (f) Energy band diagram of FTO/nc-CdS: Ag 3% device.

$$R = \frac{(I_p - I_d)}{PA}$$

$$D^* = \frac{RA^{1/2}}{(2eI_d \triangle f)^{1/2}}$$

Where I_p is the photocurrent, I_d is the dark current, P is the incident light intensity, A is the effective device area, and e is the electronic charge. For a white light source with an incident intensity of 8.5 mW cm^{-2} at zero bias operating voltage, the values for S, R, and D* were calculated using the equations provided. The estimated values obtained are as follows: S is approximately 13.82, R is approximately 0.0116 mA/W, and D* is approximately 7.39 x 10^7 Jones [18]. The performance metrics obtained for the photodetector, specifically the responsivity of approximately 0.0116 mA/W and detectivity around 7.39×10^7 Jones, are relatively low compared to typical values reported for photodetectors, including self-powered devices. The causes of the relatively low performance metrics of the photodetector can be summarized as:

(a) The relatively high series resistance of about 20 kΩ within the device, which hinders efficient carrier transport, causing internal voltage drops and lowering photocurrent extraction.

(b) The nanocrystalline CdS films having numerous grain boundaries and defect states that act as recombination centers, reducing carrier lifetime and photocurrent quantum efficiency, thereby decreasing responsivity.

(c) Imperfect carrier collection at interfaces, likely due to surface states at the FTO/nc-CdS junction and use of silver paste contacts instead of evaporated metals, which may form injection barriers limiting carrier separation effectiveness.

These factors collectively limit the device's efficiency in converting incident photons to electrical signals and reduce its signal-to-noise ratio [29]. To enhance device performance, strategies such as optimizing film quality through controlled deposition and post-annealing to minimize defects and grain boundaries, interface engineering with passivation layers or surface treatments to reduce traps and improve band alignment, and reducing series resistance using more conductive and uniform contact methods like evaporation or sputtering, are essential. Incorporating charge transport or heterojunction layers can further enhance carrier separation and collection efficiency. While the current device demonstrates proof-of-concept for self-powered photodetection, these improvements are crucial to achieve higher responsivity and detectivity in future device iterations.

To examine the ability to track a rapidly changing optical signal, which is vital for applications such as optical switching and light-wave communication [17, 30]. Further investigations were done under zero-bias conditions. In these tests, a green laser light with a wavelength of 532 nm and an intensity of 1 mW cm^{-2} was used. The laser light was modulated using a mechanical chopper, as shown in Fig. 7(a). The variation in photocurrent over time was recorded with a Digital Phosphor Oscilloscope (Model: Tektronix DPO 4054). Fig. 7(b-e) demonstrates the photocurrent response of the self-powered photodetector at light switching frequencies of 20 Hz, 100 Hz, 800 Hz, and 1000 Hz. The results show that the device operates reliably across a broad frequency range and functions effectively as a self-powered signal detector without requiring an external power source [31].

The operation of this photodetector can be explained using the energy band diagram shown in Fig. 7(f). The band gap of nc-CdS: 3% is calculated to be 2.21 eV. We reference the literature values for the band gap, conduction band minimum, and valence band maximum of FTO, as illustrated in Fig. 7(f) [32]. When these materials come into contact, electrons begin to drift from the nc-CdS: Ag 3% to the FTO until their Fermi levels align. At equilibrium, a built-in electric field forms within the depletion region at the interface of FTO and nc-CdS: Ag 3%. Similar to traditional Schottky junction solar cells, the FTO thin film is nearly transparent to visible light, allowing the nc-CdS: Ag 3% to effectively absorb photons with energy $E \geq E_g$. When illuminated, electron-hole pairs generated in the nc-CdS: Ag 3% are quickly separated; the electrons are pushed into the FTO. Due to this built-in potential, these photo-generated carriers can easily be separated and transported in opposite directions. The accumulation of these carriers on either side of the depletion region creates an open-circuit voltage. When the photodetector is short-circuited, the electrons and holes created by light can move through the external circuit, generating a current called the short-circuit current. This process helps in producing the photocurrent, which allows the device to function without needing any external power [33].

One of the key features of a photodetector is how quickly it can respond. A device with a fast response speed is ideal for

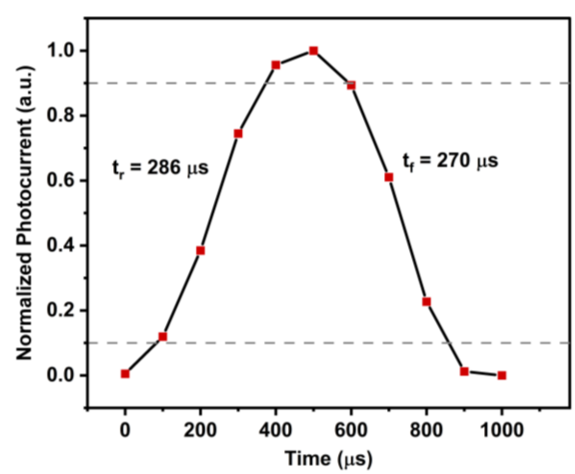

Fig. 8. Normalized photocurrent versus time plot of a single cycle at 1000 Hz, showing the rising and falling edges used to estimate the rise time and fall time.

high-speed photodetection. The response time of a photodetector is determined by two factors: rise time (t_r) and fall time (t_d). The rise time is the time it takes for the photocurrent to go from 10% to 90% of the maximum current (I_{peak}). Conversely, the fall time is the duration required for the photocurrent to decrease from 90% to 10% of I_{peak} [34]. The measured rise time and fall time for our photodetector were approximately 286 µs and 270 µs, respectively (see Fig. 8). The short rise time and fall time of our device indicate that it is a high-speed photodetector.

Conclusion

In summary, a self-powered, high-speed photodetector based on the FTO/nc-CdS: Ag 3% heterojunction has been successfully fabricated. This was achieved by depositing thin films of 3% Ag-doped nc-CdS onto an FTO-coated glass substrate using thermal evaporation with the IGC technique. The optical, electrical, and optoelectrical properties of the device were thoroughly investigated. X-ray diffraction (XRD), Raman spectroscopy, and field emission scanning electron microscopy (FE-SEM) confirm that the nc-CdS: Ag 3% thin film possesses a polycrystalline structure similar to that of bulk CdS and adequately covers the FTO-coated glass substrate. The current-voltage (I-V) measurement revealed that the heterojunction exhibits rectification characteristics in the dark and a pronounced photovoltaic effect under light illumination, with open-circuit voltage (V_{oc}), short-circuit current (I_{sc}) and fill factor (FF) of 0.022 V, 0.1064 µA, and 32.24%, respectively. To investigate the performance of the photodetector, sensitivity ($S \approx 13.82$), responsivity ($R \approx 0.0116$ mA/W), and relative detectivity ($D^* \approx 7.39 \times 10^7$ Jones) are recorded for this device using a white light source of incident intensity 8.5 mW cm^{-2} at zero bias operating voltage. It was found that the dynamic response of the device was reproducible at high frequency and recorded up to 1000 Hz. In addition, the rise time and the fall time were recorded as 286 µs and 270 µs, respectively. Outcomes of this work indicate that FTO/nc-CdS: Ag 3% heterojunction may be good candidates for optoelectronics like optical switching, light-wave communication, and next-generation visible photodetectors.

References

Arulanantham, A. M. S., Valanarasu, S., Adaikalam, K., & Jeyadheepan, K. (2018). Solution volume effect on structural, optical and photovoltaic properties of nebulizer spray deposited SnS thin films. *Journal of Materials Science: Materials in Electronics, 29*, 12899–12909. **https://doi.org/10.1007/s10854-018-9409-1**

Cao, L.-A., Yao, M.-S., Jiang, H.-J., Kitagawa, S., Ye, X.-L., Li, W.-H., & Xu, G. (2020). A highly oriented conductive MOF thin film-based Schottky diode for self-powered light and gas detection. *Journal of Materials Chemistry A, 8*, 9085–9090. **http://dx.doi.org/10.1039/D0TA01379J**

Chen, X., Song, Y., & Han, M. (2021). Portable and wearable self-powered systems based on emerging energy harvesting technology. *Microsystems & Nanoengineering, 7*, 25. **https://doi.org/10.1038/s41378-021-00248-z**

Duan, L., He, F., Tian, Y., Sun, B., Fan, J., Yu, X., Ni, L., Zhang, Y., Chen, Y., & Zhang, W. (2017). Fabrication of self-powered fast-response ultraviolet photodetectors based on graphene/ZnO:Al nanorod-array-film structure with stable Schottky barrier. *ACS Applied Materials & Interfaces, 9*, 8161–8168. **https://doi.org/10.1021/acsami.6b14305**

Farag, A. A. M., Farooq, A., & Yakuphanoglu, F. (2011). Characterization and performance of Schottky diode based on wide band gap semiconductor ZnO using a low-cost and simplified sol–gel spin coating technique. *Microelectronic Engineering, 88*, 2894–2899. **https://doi.org/10.1016/j.mee.2011.03.016**

Fiat, S., & Çankaya, G. (2012). Evaluation of the hydrostatic pressure effect on Mn/p-Si Schottky barrier diode electrical parameters and interface states. *Materials Science in Semiconductor Processing, 15*, 461–466. **https://doi.org/10.1016/j.mssp.2012.03.004**

Jang, S., Shim, H., & Yu, C. (2022). Fully rubbery Schottky diode and integrated devices. *Science Advances, 8*, eade4284. **https://doi.org/10.1126/sciadv.ade4284**

Jagani, H. S., Gupta, S. U., Bhoraniya, K., Navapariya, M., Pathak, V. M., Solanki, G. K., & Patel, H. (2022). Photosensitive Schottky barrier diodes based on Cu/p-SnSe thin films fabricated by thermal evaporation. *Materials Advances, 3*(5), 2425–2433. **https://doi.org/10.1039/D1MA01005K**

Kalsi, T., Saxena, N., & Kumar, P. (2025). Augmenting the broadband feature in CdS CQDs thin film photodetectors by Ag assimilation. *Solid State Sciences, 160*, 107805. **https://doi.org/10.1016/j.solidstatesciences.2024.107805**

Kang, J., Kotnala, R. K., & Tripathi, S. K. (2020). Effect of Sn incorporation on structural, physical and electrical properties of Ge-Se-Sb-Sn thin films. *Chalcogenide Letters, 17*, 631. **https://chalcogen.ro/631_KangJ.pdf**

Kumaar Swamy Reddy, B., Panda, S., Ramasamy, E., Badhulika, S., Veerappan, G., & Borse, P. H. (2023). Fabrication of a self-powered broadband photodetector by 50% replacement of Pb by Mg in the CH3NH3Pb0.5Mg0.5Cl2I perovskite lattice. *Materials Advances, 4*(24), 6522–6534. **https://doi.org/10.1039/D3MA00411B**

Mandal, S. K., Maity, A. B., Dutta, J., Pal, R., Chaudhuri, S., & Pal, A. K. (1997). Au/CdS Schottky diode fabricated with nanocrystalline CdS layer. *Physica Status Solidi A, 163*(2), 433–443. **https://doi.org/10.1002/1521-396X(199710)163:2%3C433::AID-PSSA433%3E3.0.CO;2-1**

Meng, Z., Jiang, Z., Zheng, Y., Shi, K., Li, J., Pan, X., & Liu, F. (2025). Self-powered photodetectors based on transition-metal dichalcogenides: A heterojunction perspective. *Frontiers of Physics, 20*, 054301. **https://doi.org/10.15302/frontphys.2025.054301**

Najm, A. S., Aljuhani, A., Naeem, H. S., Sopian, K., Ismail, R. A., Holi, A. M., Sabri, L. S., Abdullah AL-Zahrani, A., Rasheed, R. T., & Moria, H. (2022). Mechanism and principle of doping: Realizing of silver incorporation in CdS thin film via doping concentration effect. *RSC Advances, 12*, 29613–29626. **http://dx.doi.org/10.1039/D2RA04790J**

Nazir, A., Toma, A., Shah, N. A., Panaro, S., Butt, S., Sagar, R. U. R., Raja, W., Rasool, K., & Maqsood, A. (2014). Effect of Ag doping on opto-electrical properties of CdS thin films for solar cell applications. *Journal of Alloys and Compounds, 609*, 40–45. **https://doi.org/10.1016/j.jallcom.2014.04.144**

Nawaz, M. Z., Xu, L., Zhou, X., Shah, K. H., Wang, J., Wu, B., & Wang, C. (2021). CdS nanobelt-based self-powered flexible photodetectors with high photosensitivity. *Materials Advances, 2*, 6031–6046. **https://doi.org/10.1039/D1MA00580D**

Patil, G. E., Kajale, D. D., Gaikwad, V. B., & Jain, G. H. (2012). Preparation and characterization of SnO2 nanoparticles by hydrothermal route. *International Nano Letters, 2*, 17. **https://doi.org/10.1186/2228-5326-2-17**

Periyanagounder, D., Gnanasekar, P., Varadhan, P., He, J.-H., & Kulandaivel, J. (2018). High performance, self-powered photodetectors based on a graphene/silicon Schottky junction diode. *Journal of Materials Chemistry C, 6*, 9545–9551. **http://dx.doi.org/10.1039/C8TC02786B**

Ramakrishnan, K., Ajitha, B., & Ashok Kumar Reddy, Y. (2022). Review on metal sulfide-based nanostructures for photodetectors: From ultraviolet to infrared regions. *Sensors and Actuators A: Physical, 349*, 114051. **https://doi.org/10.1016/j.sna.2022.114051**

Saini, G. S. S., Sharma, A., Singh, S., Abbas, J. M., Tripathi, S. K., Kaur, S., Mahajan, C. G., Thanga, H. H., & Verma, A. L. (2007). Resonance Raman and electronic absorption study of free-base tetraphenylporphine diacid dispersed in polymethylcyanoacrylate. *Journal of Raman Spectroscopy, 38*, 1561–1569. **https://doi.org/10.1002/jrs.1802**

Saleem, M. F., Zhang, H., Deng, Y., & Wang, D. (2017). Resonant Raman scattering in nanocrystalline thin CdS film. *Journal of Raman Spectroscopy, 48*, 224–229. **https://doi.org/10.1002/jrs.5002**

Shah, N., Nazir, A., Mahmood, W., Syed, W., Butt, S., Ali, Z., & Maqsood, A. (2012). Physical properties and characterization of Ag doped CdS thin films. *Journal of Alloys and Compounds, 512*, 27–32. **https://doi.org/10.1016/j.jallcom.2011.08.081**

Sherkar, T. S., Momblona, C., Gil-Escrig, L., Ávila, J., Sessolo, M., Bolink, H. J., & Koster, L. J. A. (2017). Recombination in perovskite solar cells: Significance of grain boundaries, interface traps, and defect ions. *ACS Energy Letters, 2*(5), 1214–1222. **https://doi.org/10.1021/acsenergylett.7b00236**

Singh, B., Singh, J., Kaur, J., Moudgil, R. K., & Tripathi, S. K. (2016). Investigations of the drift mobility of carriers and density of states in nanocrystalline CdS thin films. *Physica B: Condensed Matter, 490*, 49–56. **https://doi.org/10.1016/j.physb.2016.03.006**

Singh, B., Singh, J., Kaur, R., Moudgil, R. K., & Tripathi, S. K. (2017). Quantitative measurement of transport properties: Ag-doped nanocrystalline CdS thin films. *RSC Advances, 7*, 53951–53962. **https://doi.org/10.1039/C7RA02904G**

Swanepoel, R. (1983). Determination of the thickness and optical constants of amorphous silicon. *Journal of Physics E: Scientific Instruments, 16*, 1214–1222. **https://doi.org/10.1088/0022-3735/16/12/023**

Thompson, M. T. (2014). Review of diode physics and the ideal (and later, nonideal) diode. *Intuitive Analog Circuit Design* (pp. 53–86). **https://doi.org/10.1016/B978-0-12-405866-8.00003-6**

Tombak, A., Benhaliliba, M., Ocak, Y. S., & Kiliçoglu, T. (2015). The novel transparent sputtered p-type CuO thin films and Ag/p-CuO/n-Si Schottky diode applications. *Results in Physics*, *5*, 314–321. **https://doi.org/10.1016/j.rinp.2015.11.001**

Ward, M. D., Shi, W., Gasparini, N., Nelson, J., Wade, J., & Fuchter, M. J. (2022). Best practices in the measurement of circularly polarised photodetectors. *Journal of Materials Chemistry C*, *10*, 10452–10463. **https://doi.org/10.1039/D2TC01224C**

Wang, J., Chang, Y., Huang, L., Jin, K., & Tian, W. (2018). Designing CdS/Se heterojunction as high-performance self-powered UV-visible broadband photodetector. *APL Materials*, *6*(7), 076106. **https://doi.org/10.1063/1.5042549**

Wu, D., Jiang, Y., Zhang, Y., Yu, Y., Zhu, Z., Lan, X., Li, F., Wu, C., Wang, L., & Luo, L. (2012). Self-powered and fast-speed photodetectors based on CdS:Ga nanoribbon/Au Schottky diodes. *Journal of Materials Chemistry*, *22*, 23272–23276. **https://doi.org/10.1039/C2JM34869A**

Wu, P., Dai, Y., Sun, T., Ye, Y., Meng, H., Fang, X., Yu, B., & Dai, L. (2011). Impurity-dependent photoresponse properties in single CdSe nanobelt photodetectors. *ACS Applied Materials & Interfaces*, *3*, 1859–1864. **https://doi.org/10.1021/am200043c**

Xie, C., Luo, L. B., Zeng, L. H., Zhu, L., Chen, J. J., Nie, B., Hu, J. G., Li, Q., Wu, C. Y., Wang, L., & Jie, J. S. (2012). p-CdTe nanoribbon/n-silicon nanowires array heterojunctions: Photovoltaic devices and zero-power photodetectors. *CrystEngComm*, *14*, 7222–7228. **https://doi.org/10.1039/C2CE25791B**

Khanna, S., Noor, A., Neeleshwar, S., & Tyagi, M. (2011). Effect of annealing temperature on the electrical characteristics of platinum/4H-SiC Schottky barrier diode. *International Journal of Electronics*, *98*, 1733–1741. **https://api.semanticscholar.org/CorpusID:110917230**

***